International Journal of Biological Macromolecules 295 (2025) 139669

Contents lists available at ScienceDirect

International Journal of Biological Macromolecules

journal homepage: www.elsevier.com/locate/ijbiomac

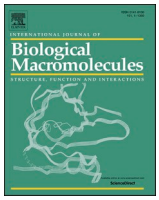

Biochemical characterization and molecular docking of a novel alkaline-stable keratinase from *Amycolatopsis* sp. BJA-103

Xia Yan [a], Hanqi Zhou [a], Ruolin Wang [a], Huan Chen [a], Bingjie Wen [a], Mengmeng Dong [a], Quanhong Xue [b], Lianghui Jia [a,*], Hua Yan [a,*]

[a] College of Life Science, Northwest A&F University, Yangling 712100, China
[b] College of Natural Resources and Environment, Northwest A&F University, Yangling 712100, China

ARTICLE INFO

Keywords:
Protease
Amycolatopsis
AlphaFold
Thermostability
Alkaline stability
Molecular docking
Molecular dynamics simulation

ABSTRACT

Amycolatopsis sp. BJA-103 was isolated for its exceptional feather-degradation capability, leading to the purification, cloning, and heterologous expression of the keratinase enzyme, KER0199. Sequence analysis places KER0199 within the S8 protease family, revealing <60 % sequence similarity to known proteases. The recombinant KER0199-His_6 demonstrates a broad substrate range, along with remarkable thermostability and alkaline stability, exhibiting optimal activity at pH 11.0 and 60 °C, despite the absence of cysteine residues essential for disulfide bonding. Structural modeling reveals a predominantly negatively charged surface and a flat, low-electrostatic-potential substrate-binding pocket. Substrate-binding models, predicted using AlphaFold3 and molecular dynamics simulations, indicate that substrates such as casein, chicken feather β-keratin P2450, and hemoglobin bind to this pocket, forming anti-parallel β-sheets with residues G97 to G99 and establishing extensive hydrogen bonds with key residues near the enzyme's active site. These findings suggest that AlphaFold-based substrate binding predictions, combined with an analysis of intermolecular forces, provide a valuable tool for assisting in the elucidation of enzyme specificity and substrate recognition. KER0199, the first characterized S8 family keratinase from the *Amycolatopsis* genus, shows great potential for industrial applications.

1. Introduction

The rapid expansion of global livestock farming has led to the accumulation of keratin-rich by-products, including chicken feathers, pig bristles, wool, and horns. Managing these by-products presents significant challenges and raises environmental concerns [1–3]. Keratins are highly resistant to degradation due to their extensive disulfide cross-linking, hydrophobic interactions, and hydrogen bonding, which make them difficult to break down using conventional enzymes such as papain, pepsin, and trypsin [4,5].

Efficient keratin degradation can convert these by-products into valuable proteins and amino acids, which are beneficial for various applications including animal feed, fertilizers, detergents, leather and textile industries, and pharmaceuticals [6]. Although traditional methods such as alkaline hydrolysis and vapor pressure are effective for feather degradation, they destroy essential amino acids (e.g., methionine, lysine, and histidine) and often involve high costs and environmental risks [7]. In contrast, microbial hydrolysis using keratinases offers a more sustainable and environmentally friendly alternative [4]. Keratinases, primarily serine proteases or serine metalloproteases, have unique catalytic properties that improve their efficiency [8,9]. They belong to various MEROPS protease families, such as S08, M03, M14, M28, and M36, with the S08 family being particularly prominent for keratin degradation [10,11]. >30 classes of microorganisms, including bacteria and fungi, have demonstrated significant keratinolytic activity [9]. *Bacillus* spp. and keratinophilic fungi are well-documented for their keratinase production, but scaling up keratinase applications remains a challenge [12]. Many available enzymes are unsuitable for industrial use, highlighting the need for highly active and robust enzymes that can withstand diverse pH and temperature conditions [11]. The discovery and development of keratinases with higher efficiency and improved tolerance to harsh conditions is a major research focus [13–17]. Genetic engineering techniques, such as site-directed mutagenesis of wild-type enzymes and the use of modified promoters, have successfully enhanced the substrate specificity, yield, activity, and stability of keratinases [15]. These efforts have also resulted in several patents. For

* Corresponding authors.
E-mail addresses: yanxia@nwafu.edu.cn (X. Yan), jialianghui@nwafu.edu.cn (L. Jia), yanhua@nwafu.edu.cn (H. Yan).

https://doi.org/10.1016/j.ijbiomac.2025.139669
Received 2 September 2024; Received in revised form 8 December 2024; Accepted 7 January 2025
Available online 8 January 2025

example, Patent No. CN111662908 and US11384349B2 describe efficient keratinase expression in *Bacillus* recombinant strains through promoter modification and plasmid engineering, respectively [18,19]. Additionally, Patent CN106636042 demonstrates significant improvements in the thermal stability and enzymatic activity of keratinase through site-directed mutagenesis [20]. These advancements underscore the growing importance of keratinases in industrial applications, extending their utility beyond basic research.

The properties of keratinolytic proteases vary depending on the producing organism; keratinases produced by different strains may be suitable for various industrial processes and applications [9].The genus *Amycolatopsis* is a rare group of soil-dwelling Actinomycetotas that also exhibit endophytic capabilities in crops [21]. Within this genus, *Amycolatopsis keratiniphila* $D2^T$ has been recognized for its exceptional keratin degradation activity [22,23]. However, only two S1 family keratinases have been characterized in this strain so far, and detailed characterization of keratinases from this genus is still limited [23]. In this study, a strain, BJA-103, was isolated from the *Valeriana* rhizosphere and identified as a novel strain of *Amycolatopsis* sp.. This strain demonstrates remarkable feather degradation capabilities, suggesting its potential for addressing keratin waste. The keratinase KER0199 was purified and characterized, providing valuable insights into its structure and function, and highlighting its unique properties and potential applications in waste management and industrial processes.

2. Materials and methods

2.1. Chemicals, strains, plasmids, and medium cultures

All chemicals were of analytical grade. *E. coli* DH5α was used for routine cloning, while *E. coli* S17–1 was used for conjugative transfer. *Streptomyces pactum* Act12, preserved in the laboratory, was used for heterologous expression of KER0199. The plasmid used for conjugative transfer was a derivative of pSET152::*PermE** constructed in the laboratory [24], featuring the erythromycin resistance gene promoter, a strong promoter commonly used in *Streptomyces*.

Luria-Bertani (LB) liquid medium (10 g/L Tryptone, 5 g/L Yeast extract, 5 g/L NaCl) was used for bacterial cultivation. GAUZE's NO.1 medium (20 g/L soluble starch, 1 g/L KNO_3, 0.5 g/L NaCl, 0.5 g/L K_2HPO_4, 0.5 g/L $MgSO_4{\cdot}7H_2O$, 0.01 g/L $FeSO_4{\cdot}7H_2O$, 15 g/L agar) was used for cultivating *Amycolatopsis*. Liquid Tryptic Soy Broth (TSB) medium (17 g/L Tryptone, 3 g/L Soybean peptone, 5 g/L NaCl, 2.5 g/L K_2HPO_4, 2.5 g/L Glucose) was used for seed culture. Milk agar medium (5 g/L skimmed milk powder, 15 g/L agar) was used for screening target strains. 2CMY medium (10 g/L soluble starch, 2 g/L tryptone, 1 g/L NaCl, 2 g/L $(NH_4)_2SO_4$, 1 g/L K_2HPO_4, 2 g/L $CaCO_3$, 1 g/L KNO_3, 0.001 g/L $FeSO_4{\cdot}7H_2O$, 0.001 g/L $MgCl_2{\cdot}6H_2O$, 0.001 g/L $ZnSO_4{\cdot}7H_2O$, 15 g/L agar) was used for conjugative transfer. The feather medium for keratinase production contained 10 g/L natural chicken feathers, 0.5 g/L NaCl, 0.7 g/L K_2HPO_4, and 0.35 g/L KH_2PO_4.

2.2. Identification of the strain BJA-103

Strain BJA-103 was selected for its significant ability to degrade both casein and feathers. Morphological and genetic identifications were performed according to *the Manual of Classification and Identification of Actinomycetes* and 16S rDNA sequencing [25]. The 16S rDNA gene was amplified using primers 27F (5'-AGAGTTTGATCCTGGCTGAG-3′) and 1522R (5'-AAGGAGGTGATCCAGCCGCA-3′). The thermal cycling conditions were as follows: initial denaturation at 95 °C for 5 min, followed by 32 cycles of denaturation at 95 °C for 10 s, annealing at 57 °C for 5 s, extension at 72 °C for 10 s, and a final extension at 72 °C for 5 min. The PCR product was cloned into the pMD™19-T vector (Takara, Japan) and sequenced by Sangon Biotech (Shanghai, China). The sequence was analyzed using Nucleotide BLAST, and a neighbor-joining phylogenetic tree was constructed using MEGA11 [26].

2.3. Scanning electron microscopy of strain BJA-103

Strain BJA-103 was cultured on GAUZE's NO.1 Medium at 28 °C for 5 days. Cultured areas exhibiting growth were harvested, soaked overnight at 4 °C in 2.5 % glutaraldehyde, and then washed twice with water. The cells were subjected to gradient dehydration using ethanol (30 %, 50 %, 70 %, 90 %, and 100 %), were air-dried, then coated with platinum, and examined using an S-3400 N scanning electron microscope (Hitachi, Japan).

2.4. Feather-degrading ability of strain BJA-103

To evaluate the feather-degrading ability of strain BJA-103, 250 mL Erlenmeyer flasks containing 10 g/L native feathers in 50 mL feather medium were inoculated with 5 % (*v*/v) of the bacterial culture. The flasks were incubated under static and shaking (180 rpm) conditions for various time intervals, as described by Abdel-Fattah et al. [7]. Feather-degrading efficiency was assessed by measuring the degree of feather degradation through visual inspection and biochemical assays.

2.5. Purification and identification of native keratinase from strain BJA-103

The keratinase enzyme was purified following standard procedures [8]. The cell-free culture supernatant, collected after 120 h of cultivation, was precipitated with 80 % saturated ammonium sulfate and incubated overnight at 4 °C. The mixture was then centrifuged at 12,000 ×*g* for 10 min at 4 °C. The precipitate was dissolved in 20 mM Tris-HCl buffer (pH 7.0) and dialyzed at 4 °C for 12 h, with buffer changes every 4 h.

The dialyzed sample was loaded onto a diethylaminomethyl (DEAE)-cellulose column equilibrated with 20 mM Tris-HCl buffer (pH 7.0) and eluted with a linear gradient of NaCl (0.2 M, 0.5 M, and 0.8 M, each in 200 mL) in the same buffer. Fractions (15 mL) were collected and analyzed for protein concentration and enzyme activity. The molecular weight of the active protein was estimated using sodium dodecyl sulfate-polyacrylamide gel electrophoresis (SDS-PAGE).

Active fractions were dialyzed and concentrated with PEG 2000 at 4 °C. The concentrated protease was electrophoresed on a 12 % non-denaturing polyacrylamide gel, which was then cut into two parts. One part was treated with Tris-HCl buffer (pH 8.0) containing Triton X-100, incubated in 20 g/L casein at 40 °C for 3 h, stained with Coomassie Brilliant Blue, and decolorized overnight. The other part was directly stained and decolorized. The keratinase activity was confirmed by comparing the two gel parts. Active bands were excised and analyzed by nano-high performance liquid chromatography-electrospray ionization mass spectrometry (nanoHPLC-ESI-MS)/MS at Beijing Baitai Park Biotechnology Co., Ltd. (Beijing, China). The partial amino acid sequence was used to identify the coding gene, designated as KER0199, by aligning it with the BJA-103 genome sequence.

2.6. Heterologous expression and purification of KER0199 in Streptomyces pactum Act12

KER0199 was expressed in *Streptomyces pactum* Act12 via conjugation with *E. coli* S17–1. The KER0199 gene was amplified by polymerase chain reaction (PCR) using primers 5'-GGATCCAGGAAGGGAACCAGTGAGCAAG-3′ (forward, ribosomal binding site underlined) and 5′-TCTA-GATCAATGATGATGATGATGCTTCACCTGGAGCAGCTTGTTC -3′ (reverse, His_6-tag underlined). The PCR product was digested with BamHI and *Xba*I and ligated into the pSET152::PermE* plasmid. The resulting plasmid, pSET152::PermE::KER0199, was introduced into *Streptomyces pactum* Act12 via conjugative transfer from *E. coli* S17–1. Positive transformants were selected based on apramycin resistance, and confirmed by amplifying the apramycin resistance gene using primers

5'-GTGCAATACGAATGGCGAAAAGC-3′ (forward) and 5'-TCAGCCAATCGACTGGCGAGC-3′ (reverse), after three generations on apramycin (10 μg/mL) and non-antibiotic plates.

2.7. Determination of enzymatic activity of recombinant keratinase KER0199-His$_6$

The enzymatic activity of keratinase was assessed with modifications to the protocol described by Yamamura et al. [27]. Soluble keratin was purchased from Tokyo Chemical Industry (Japan). The reaction mixture, consisting of 100 μL of 10 g/L soluble keratin and 100 μL of purified recombinant keratinase solution (0.012 mg/mL in 20 mM Tris-HCl, pH 7.9), was incubated at 40 °C for 3 h. To terminate the reaction, 60 g/L trichloroacetic acid was added, and the mixture was further incubated at 40 °C for 20 min to ensure complete precipitation of any unreacted substrate. After centrifugation at 4 °C, 16,000 ×g for 10 min, the supernatant was collected. To 100 μL of supernatant, 0.5 M Na_2CO_3 was added to neutralize the sample, followed by 100 μL of Folin-Phenol reagent. The mixture was then incubated at 40 °C for 20 min and subsequently cooled in water. Keratinase activity was quantified by measuring the absorbance at 660 nm. The keratinolytic activity was quantified in keratin units (U), defined as an increase of 0.01 absorbance at 660 nm within 1 h. All experiments were performed in triplicate, and the results are presented as mean ± SD.

2.8. Effect of temperature and pH on activity of recombinant keratinase KER0199-His$_6$

The effect of temperature on the purified His-tagged keratinase was assessed by incubating the reaction mixture at temperatures ranging from 40 °C to 80 °C for 1 h at pH 10. The optimal pH was determined by conducting the enzyme reaction at pH values between 7.0 and 12.0 for 1 h at the identified optimal temperature. Thermal stability of the recombinant keratinase was evaluated by pre-incubating the enzyme in buffer (without substrate) at temperatures from 30 °C to 80 °C for 1 h. The buffer used was 20 mM Tris-HCl at pH 7.9, prepared by dissolving 2.42 g of Tris in 900 mL of deionized water. The pH was adjusted to 7.9 using concentrated hydrochloric acid, and the final volume was adjusted to 1000 mL with deionized water. The solution was then filtered through a 0.45 μm membrane filter and stored for future use.

2.9. Substrate specificity of recombinant keratinase KER0199-His$_6$

The substrate specificity of keratinase KER0199-His$_6$ was evaluated using both soluble and insoluble substrates. Soluble substrates, including casein, hemoglobin, and bovine serum albumin, were each dissolved at 20 mg/mL in 1 mL of 20 mM Tris-HCl buffer (pH 7.0). For insoluble feather powder, a mixture containing 20 mg of each substrate, 0.2 mL of the protein sample, and 1.8 mL of 20 mM Tris-HCl buffer was incubated at 37 °C on an orbital shaker at 180 rpm for 2 h. β-Mercaptoethanol and dithiothreitol (DL-DTT) were added to 10 μL/mL concentration each. After incubation, the supernatant was collected, and enzymatic activity was assessed using Na_2CO_3 and Folin-Ciocalteu phenol reagent. Each assay was performed in triplicate to ensure reproducibility.

2.10. Bioinformatics analysis of KER0199

The amino acid sequence of KER0199 was analyzed using SignalP-5.0 to predict the presence and location of the signal peptide (https://services.healthtech.dtu.dk/services/SignalP-5.0/). InterPro was employed to identify precursor peptides and classify the enzyme family (https://www.ebi.ac.uk/interpro/). ExPASy tools were used to estimate the mature enzyme's molecular weight, isoelectric point, and instability index (https://web.expasy.org/protparam/). Conservation analysis was conducted using ConSurf (https://consurf.tau.ac.il/consurf_index.php). Sequence homology searches were performed using NCBI BLAST (https://blast.ncbi.nlm.nih.gov/Blast.cgi).

2.11. Homology modeling and molecular docking of KER0199 with feather keratin

KER0199 was modeled using two approaches: traditional homology modeling via the Swiss-Model protein structure prediction server (http://swissmodel.expasy.org/interactive) and direct modeling using the AlphaFold3 server [28]. In the homology modeling approach, the structure of subtilisin-like serine proteinase from *Vibrio* sp. PA-44 (PDB ID: 1S2N) (X-ray, 1.5 Å resolution) was used as the template. KER0199 shared 97 % sequence coverage and 59.85 % sequence identity with 1S2N. Molecular docking was performed using the AlphaFold3 server. The PyMOL Molecular visualization software (http://www.pymol.org) was used to analyze the receptor-ligand complex further.

2.12. Molecular dynamics (MD) simulation

The complexes of KER0199 and chicken feather keratin (P2450) were simulated for 100 ns using GROMACS 2022 with the Amber99sb-ildn force field. Water was added to the system using the SPCE model, and a water box of size $10 \times 10 \times 10\ nm^3$ was created, with the box edge at least 1.2 nm away from the protein surface. Na^+ and Cl^- ions were added to balance the system automatically. The Particle-Mesh Ewald (PME) method was used to handle electrostatic interactions, and energy minimization was performed using the steepest descent algorithm with a maximum of 50,000 steps. The cutoff distances for Coulombic interactions and van der Waals interactions were both set to 1 nm. The system was then equilibrated in the NVT (canonical) and NPT (isothermal-isobaric) ensembles, followed by a 100 ns MD simulation at constant temperature and pressure. Nonbonded interactions were truncated at 10 Å. The temperature was controlled at 300 K using the V-rescale temperature coupling method, and pressure was maintained at 1 bar using the Berendsen method. Finally, GROMACS tools (gmx rmsd, gmx rmsf, gmx hbond, and gmx MMPBSA) were used to analyze the root-mean-square deviation (RMSD), root-mean-square fluctuation (RMSF), hydrogen bonds, and binding free energy, respectively.

3. Results and discussion

3.1. Identification and feather-degrading capability of strain BJA-103

Strain BJA-103, isolated from the rhizosphere of *Valeriana jatamansi* Jones, demonstrated significant degradation of native chicken feathers within five days (Fig. 1a, b). Scanning electron microscopy (SEM) images after a 5-day incubation at 28 °C on Gauze's No. 1 medium revealed the formation of irregularly shaped fragments (Fig. 1c). Phylogenetic analysis of 16S rDNA sequences placed strain BJA-103 within a clade that includes three species of the genus *Amycolatopsis*, with a bootstrap support of 100 % (Fig. 1d), thereby confirming that BJA-103 belongs to the genus *Amycolatopsis*.

3.2. Purification of native keratinase KER0199 and identification of its coding gene

Given the exceptional keratin-degrading capability of strain BJA-103, the focus was placed on characterizing its keratinase. The enzyme was purified through ammonium sulfate precipitation followed by column chromatography. The peaks corresponding to enzyme activity and protein concentration from the elution profile were selected for SDS-PAGE analysis. The electrophoresis results for the 16th and 28th fractions revealed two distinct protein bands (Fig. 2a, lane 4 and lane 5). Zymogram analysis demonstrated that only the upper band exhibited proteolytic activity (Fig. 2b, lane 2). This activity was partially inhibited by dimethyl sulfoxide (DMSO) and completely inhibited by

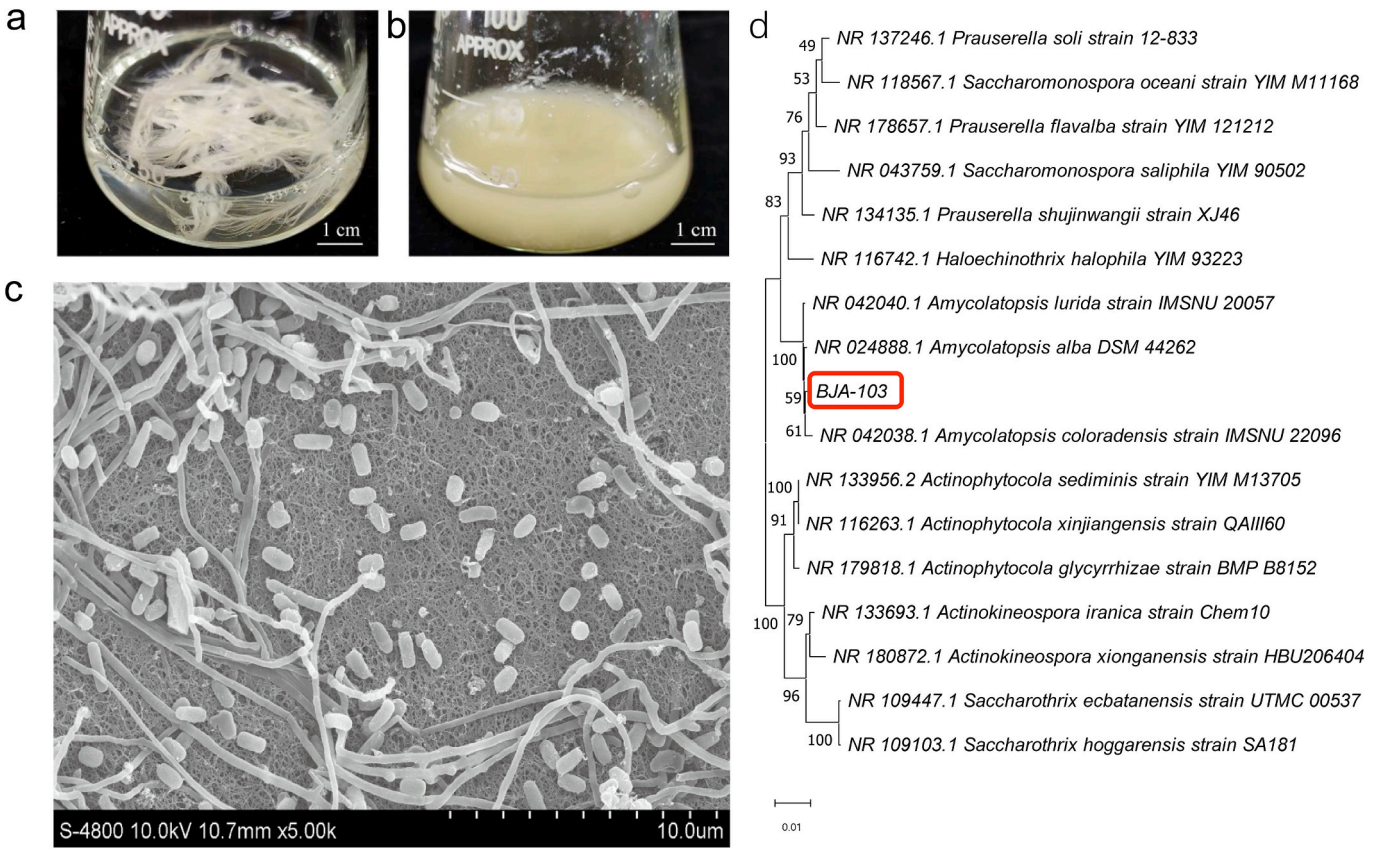

Fig. 1. Feather Degradation and Identification of Strain BJA-103.
(a) Control group without bacterial inoculation.
(b) Experimental group inoculated with strain BJA-103, showing complete degradation of native chicken feathers within 5 days. The experiment was conducted at 28 °C with a 5 % inoculum of a 48-h-old culture, shaken at 180 rpm.
(c) SEM images of mycelium growth on Gauze's No. 1 medium at 28 °C for 5 days, showing the formation of squarish fragments. Scale bar = 1 μm.
(d) Phylogenetic tree constructed using the Neighbor-Joining method, illustrating the relationship between strain BJA-103 and other selected Actinomycetotas.

phenylmethylsulfonyl fluoride (PMSF) (Fig. 2b, lanes 3 and 4). The proteins from the active upper band were sequenced using nano HPLC-ESI-MS/MS after gel extraction. Sequence alignment with the BJA-103 genome facilitated the identification of the corresponding coding genes and the complete protein sequence.

3.3. Sequence analysis of keratinase KER0199

The purified keratinase, designated KER0199, is encoded by a 1251 bp nucleotide sequence in the BJA-103 genome, resulting in a 416-amino-acid polypeptide. SignalP-5.0 and InterPro analysis indicate that the signal peptide spans residues 1 to 40, while the precursor peptides extend from residues 41 to 144 (Fig. 2c). The mature enzyme, composed of 271 amino acids, is classified as a subtilisin-like serine protease in the S8 family. This classification is supported by the enzyme's partial inhibition by DMSO and complete inhibition by PMSF (Fig. 2b, lanes 2 and 3); and its typical Asp33-His66-Ser218 catalytic triad.

ExPASy analysis estimates the molecular weight of mature KER0199 to be approximately 27,049.51 Da with a theoretical isoelectric point (pI) of 4.70. The enzyme is rich in acidic residues, particularly aspartic acid, with 28 aspartic acid and 6 glutamic acid residues. It lacks cysteines and thus cannot form disulfide bonds. The Instability Index is 6.39, indicating high stability, while the Aliphatic Index of 74.28 suggests significant thermal stability.

Conservation analysis conducted using the ConSurf server indicates that KER0199 has a compact S8 family structure characterized by α-helices and β-sheets. Conserved residues are mainly around the catalytic triad, while surface regions show lower conservation (Fig. 2d, e). NCBI BLAST analysis reveals that KER0199 homologs are present in several *Amycolatopsis* strains with over 93 % sequence homology, notably WP_083715709.1 and WP_126735511.1, although these homologs remain uncharacterized. Compared to other S8 family proteases, KER0199 shows lower homology (below 60 %) and only 34 % similarity to KerA, suggesting it is a distinctive member of the S8 family with potentially unique properties.

3.4. Expression and purification of recombinant keratinase KER0199-His_6 in *Streptomyces pactum* Act12

Heterologous expression and affinity purification are crucial for optimizing protein yield and purity for enzyme characterization. While attempts to express KER0199 in *Escherichia coli* and *Pichia pastoris* were unsuccessful, expression in *Streptomyces pactum* Act12 proved successful. In this system, the polypeptide was correctly processed, yielding the active recombinant enzyme KER0199-His_6. The enzyme demonstrated effective degradation of natural chicken feathers within 5 days (Fig. 3a). KER0199-His_6 was purified using nickel affinity chromatography, and SDS-PAGE analysis confirmed high purity, evidenced by a single band at approximately 27 kDa (Fig. 3b), affirming its suitability for further research.

3.5. Enzymatic properties of recombinant keratinase KER0199-His_6

As shown in Fig. 3c, recombinant keratinase KER0199-His_6 exhibits significant activity across a broad pH range from 7.0 to 12.0, with peak

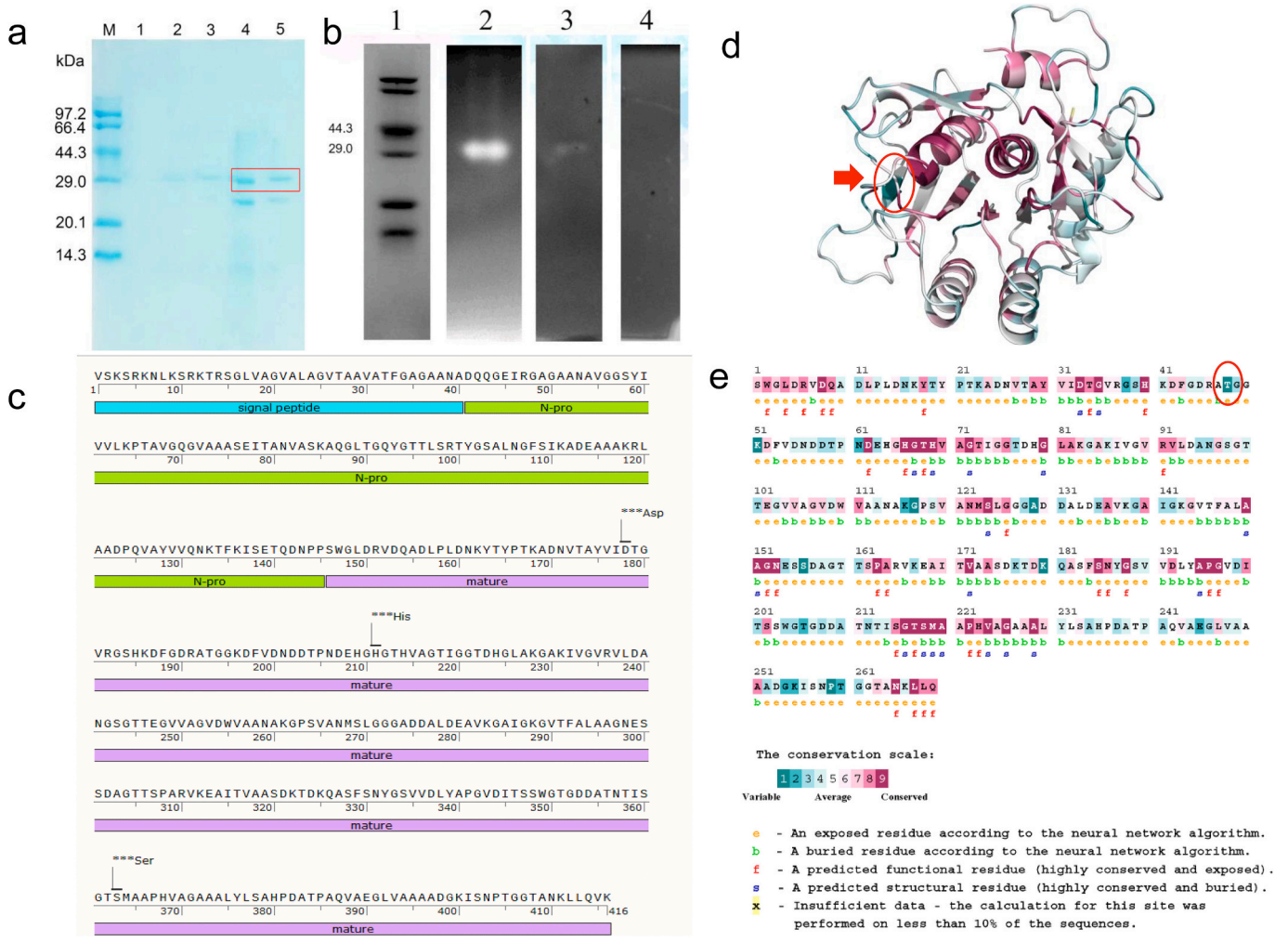

Fig. 2. Purification of native KER0199 and analysis of its coding sequence.
(a) SDS-PAGE analysis of protein components from each purification step. M is the protein molecular weight marker; Lanes 1–5 represent different fractions collected during column chromatography. The target band is highlighted within the red box.
(b) Zymogram analysis of the purified KER0199 protein: Lane 1 is the protein molecular weight marker; Lane 2 shows a bright band indicative of casein degradation; Lanes 3 and 4 demonstrate partial inhibition of proteolytic activity by DMSO and complete inhibition by PMSF, respectively.
(c) Amino acid sequence of KER0199: blue indicates the signal peptide, green represents precursor peptides, and purple denotes the mature enzyme.
(d) and (e) Conservation analysis of amino acid residues in KER0199 performed using the Consurf server. Different colors represent varying levels of conservation. (d) Conservation of different amino acid residues is shown in the 3D structure of KER0199. The red ellipses and arrows indicate amino acid residues (47 A, 48 T, 49G) that show divergence between the Swiss-Model homology model and the AlphaFold3 predicted structure mentioned in section 3.6.1. (e) Different colors in the coding sequence of the mature enzyme indicate the conservation levels of amino acid residues.

activity at approximately pH 11.0 (Fig. 3c). This alkaline pH optimum classifies the enzyme as an alkaline protease, suggesting its potential for applications in high pH environments.

Regarding thermal stability, the enzyme maintains optimal activity at approximately 60 °C, as illustrated in Fig. 3d. It retains over 80 % of its activity after preincubation at this temperature for 1 h, indicating substantial thermal stability. However, its activity diminishes significantly when exposed to 70 °C for 1 h (Fig. 3e).

Alkaline conditions facilitates keratin degradation by converting cystine residues in keratin to lanthionine, which weakens the keratin structure and makes it more susceptible to hydrolysis by keratinases [29]. Therefore, alkaline keratinases are valuable for their effectiveness in such conditions. The superior thermal stability and alkaline tolerance of KER0199 make it particularly suitable for applications in leather processing and detergent formulation, where both high pH and elevated temperatures are common [30,31].

3.6. *Substrate specificity of the recombinant keratinase KER0199-His$_6$*

As shown in Table 1, recombinant keratinase KER0199-His$_6$ exhibits a broad range of proteolytic activities across various substrates. It demonstrates the highest activity on soluble casein, which is used as a reference with 100 % normalized activity. The enzyme also significantly degrades hemoglobin, with a degradation rate of 96.72 %. In contrast, its ability to degrade bovine serum albumin (BSA) is relatively low, at only 18.79 %. The degradation activity is relatively lower for the insoluble protein feather powder, at 38.18 %. However, the presence of reducing agents such as mercaptoethanol or dithiothreitol (DL-DTT) substantially enhances KER0199-His$_6$'s ability to degrade this substrate. Specifically, the relative activity towards feather powder improved 1.69-fold with mercaptoethanol and 1.83-fold with DTT. This enhancement underscores the role of reducing agents in breaking disulfide bonds, facilitating the keratinolytic process by loosening the keratin structure. To effectively obtain amino acids from keratin-rich materials using keratinolytic enzymes, preliminary degradation of

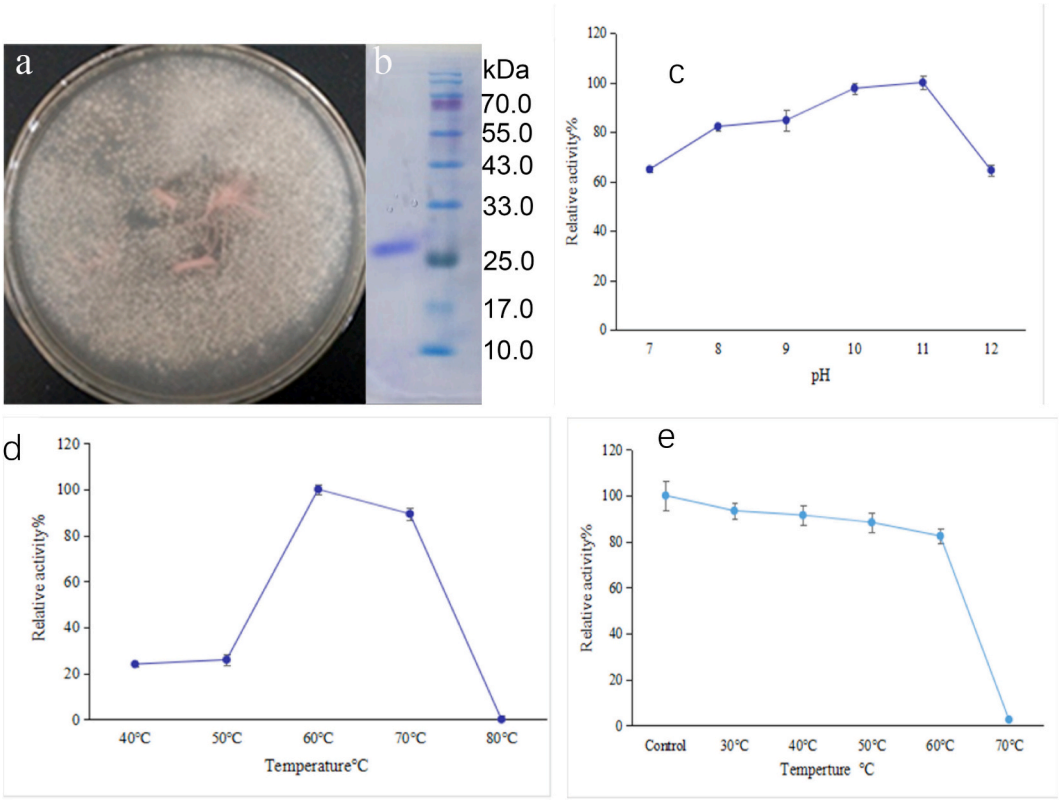

Fig. 3. Heterologous Expression and Enzymatic Properties of Recombinant KER0199 Keratinase.
(a) Degradation of natural chicken feathers by recombinant *Streptomyces pactum* Act12 over 5 days, as shown in the culture dish images.
(b) Purification of His-tagged KER0199 keratinase using nickel affinity chromatography, with detection via SDS-PAGE.
(c) Determination of the optimum pH for KER0199-His_6 activity, assessed by measuring enzyme activity at pH values ranging from 7.0 to 12.0 for 1 h at the optimum temperature.
(d) Effect of temperature on the activity of KER0199-His_6, with reactions conducted at temperatures ranging from 40 °C to 80 °C for 1 h at pH 10.
(e) Thermal stability of KER0199-His_6, evaluated by pre-incubating the enzyme (without substrate) at temperatures from 30 °C to 80 °C for 1 h.

Table 1
Substrate specificity of KER0199-His_6, showing activity with different substrates.

Substrate	Specific activity (U/mg)	Relative activity (%)
Casein	55.87 ± 1.71	100
bovine serum albumin (BSA)	10.50 ± 0.37	18.79
Hemoglobin	54.03 ± 1.68	96.72
Feather powder	21.33 ± 1.23	38.18
Feather (+β-Mercaptoethanol)	36.06 ± 1.879	64.54
Feather (+DTT)	39.06 ± 0.867	69.91

disulfide bonds is necessary to loosen the keratin structure and make the amino acid chains accessible for keratinase action [32].

Disulfide bond cleavage is commonly facilitated by disulfide reductases or reducing agents like sodium sulfide, DTT, mercaptoethanol, glutathione, cysteine, and thioglycolic acid [33]. Although KER0199 lacks internal disulfide bonds, it remains highly stable and active, suggesting that reducing agents do not significantly impact its performance during keratin degradation.

Keratinases are widely found in bacteria and fungi. The biochemical properties of keratinases from different sources vary greatly [13]. They vary mainly in terms of enzyme structure, composition, stability, optimum temperature, and optimum pH. The molecular weight of keratinase ranges from 18 to 240 kDa, but most keratinases have molecular weights between 25 and 50 kDa. Most keratinases prefer an alkaline reaction environment, with an optimal pH of approximately 7–10, and the optimal temperature for the reaction ranges from 30 to 60 °C [13]. In this study, KER0199 demonstrated stability at temperatures up to 60 °C, with an optimal pH of 11.0, indicating that it is a relatively stable protease.

The use of the Folin-Ciocalteu method for assessing protease activity is based on its fundamental principle of measuring the blue complex formed when reducing substances react with the Folin reagent. Consequently, the composition of the substrate and the ability of the hydrolyzed products to react with the Folin reagent can significantly influence the accurate determination of enzyme activity. Furthermore, various studies frequently employ different substrates to evaluate keratinase activity, such as azokeratin, keratin azure, human hair, cow horn, feathers, and keratin powder derived from various keratins [1,34]. Additionally, multiple detection techniques have been utilized [1] , making it challenging to compare the enzymatic activities of keratinases across different studies. The K:C ratio (keratinolytic activity to caseinolytic activity) has been proposed as a parameter to assess an enzyme's potential as a keratinase, serving as a standard to distinguish keratinases from conventional proteases [35]. A hydrolase with a K:C ratio >0.5 is considered a potential keratinase, while a K:C ratio below 0.5 indicates a non-keratinase. In the presence of a reducing agent, the K:C value of KER0199 exceeds 0.6, confirming its classification as a keratinase.

3.7. Modeling of KER0199 and comparison with its homologous proteins

3.7.1. Modeling of KER0199

Structural predictions of the KER0199 protease were performed using two methods: AlphaFold3 and SWISS-MODEL. For SWISS-MODEL, PDB entry 1S2N was used as the template. The resulting model demonstrated high overall quality, with a QMEANDisCo Global score of

0.83 ± 0.05, indicating good structural accuracy. The model also showed a predicted local similarity of 1.0. The MolProbity Score of 1.90 suggests excellent stereochemical quality, and the Clash Score of 1.64 indicates minimal steric clashes. Additionally, Ramachandran plot analysis revealed that 93.96 % of residues are in favored regions, with only 0.75 % in disallowed regions, highlighting the model's excellent alignment with the target structure. The structural model of KER0199, along with its comparison to the template 1S2N and the effectiveness of model evaluation, is shown in Fig. S1 of the supplementary materials.

AlphaFold3 evaluates the accuracy of predicted structures using several metrics, including the predicted local distance difference test (pLDDT), predicted aligned error (PAE), predicted template modeling (pTM), and the interface predicted template modeling (ipTM) [28]. Higher pLDDT values indicate greater confidence, while higher PAE values reflect larger predicted errors. A pTM score above 0.5 suggests reliable overall folding, and ipTM scores above 0.8 indicate high-quality predictions of subunit positioning. The AlphaFold3-predicted structure of KER0199 achieved a pLDDT score above 90 and a pTM score of 0.97 (see Fig. S2a), demonstrating strong prediction reliability.

Both SWISS-MODEL and AlphaFold3 produced structurally consistent models overall. However, a notable discrepancy was observed at residues A47, T48, and G49 (see Fig. S3). SWISS-MODEL predicted these residues to adopt a partial β-sheet conformation, consistent with the β-sheet structure inferred from the template protein (PDB ID: 1S2N). In contrast, AlphaFold3 predicted these residues to form a loop structure. This difference highlights the intrinsic variations between the two modeling approaches, which may arise from differences in how each method handles regions with alternative conformations.

For the subsequent molecular docking studies, the AlphaFold3 model was selected based on several considerations. Firstly, the accuracy of SWISS-MODEL can be limited by the similarity to its template. In contrast, AlphaFold3, leveraging advanced deep learning algorithms, may provide more detailed insights, particularly in regions that diverge from the template. Moreover, as shown in Fig. 2d, the three residues (47 A,48 T,49G) exhibit the lowest conservation in KER0199, with the corresponding residues in 1S2N being (46S,47V,48S). Additionally, the AlphaFold3-predicted structure achieved a pLDDT score exceeding 90 and a pTM score of 0.97(See Fig.S2a), indicating a high level of prediction reliability. Therefore, the subsequent structural analyses and docking are based on the AlphaFold3-predicted model.

3.7.2. *Prediction of potential calcium ion binding sites in KER0199*

The AlphaFold3 server was used to simulate the docking of multiple calcium ions to identify potential binding sites. High ipTM and pTM scores of 0.96 and 0.97, respectively, were obtained (See Fig.S2b), indicating a high degree of structural compatibility between the calcium ions and the predicted binding sites on KER0199. Additionally, as illustrated in Fig. 4, according to the simulation results, the shortest distances between the calcium ions and key residues—D5, Q9, D15, and K17 at Binding Site 1; K167, A169, and D192 at Binding Site 2; and D52, D55, D57, and T59 at Binding Site 3—are all within 2.6 Å, further validating the reliability of the AlphaFold3 predictions. The presence of bound calcium ions, characteristic of the subtilisin-like protease superfamily, is essential for correct folding and structural stability [9,36]. Since KER0199 does not possess disulfide bonds, the coordination of multiple metal ions likely contributes to its enhanced thermostability [14,37].

3.7.3. *Comparative analysis of the structure of KER0199 with 1S2N,4DZT and 5WSL*

Among the proteins with known crystal structures in the PDB database, 1S2N, 4DZT, and 5WSL exhibit high sequence identity with

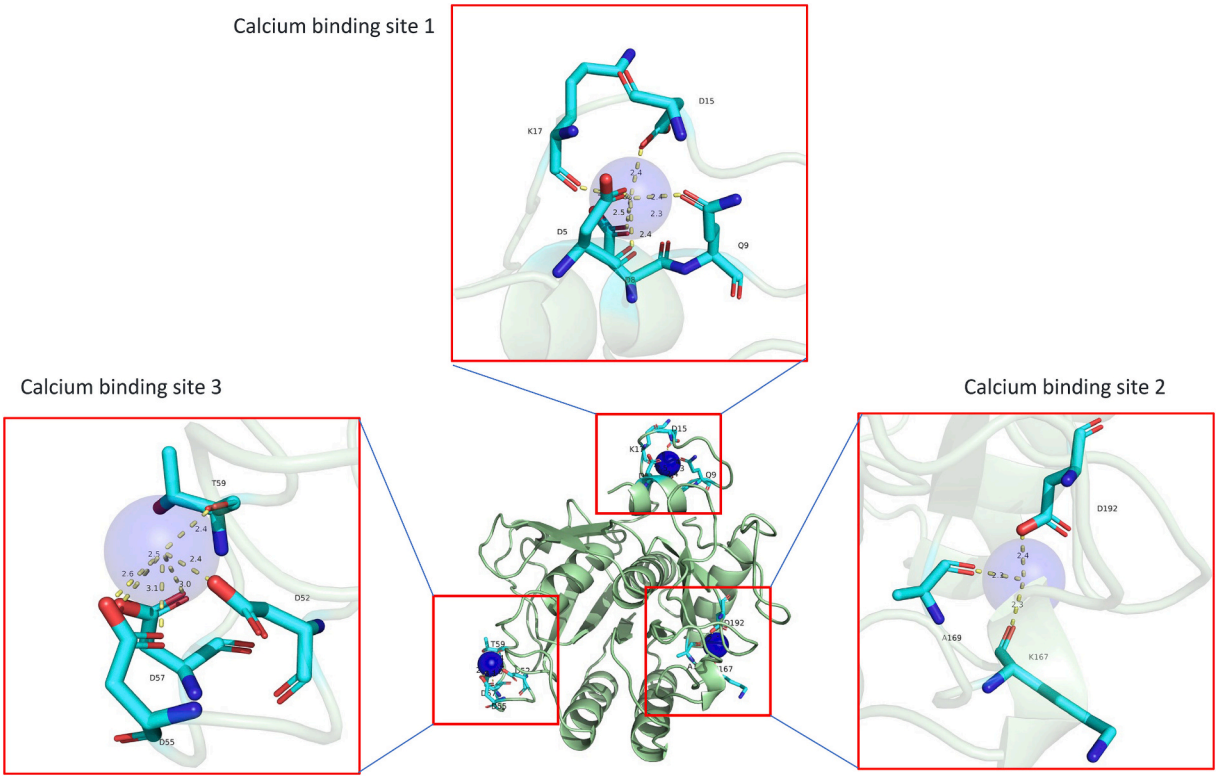

Fig. 4. Potential Calcium Ion Binding Sites in KER0199 Predicted by AlphaFold3.
Schematic representation of the three calcium ion binding sites in KER0199, predicted by AlphaFold3. KER0199 is shown in a cartoon representation. Calcium ions are depicted as blue spheres, while the nearby amino acid residues are displayed in a ball-and-stick model. Red boxes highlight and magnify the distances between the calcium ions and these amino acid residues.
The figures were prepared using PyMOL.

KER0199, with identities of 59.85 %, 57.36 %, and 56.72 %, respectively. The three proteins are all known for their exceptional stability. Interestingly, 1S2N is recognized for its cold adaptation [38], while 4DZT and 5WSL are noted for their heat stability [39,40]. This difference in environmental adaptation and stability prompted us to compare their structural and electrostatic properties with those of KER0199.

As shown in Fig. 5, despite significant sequence differences, the four proteins exhibit highly similar overall structures, characterized by the S8 family's typical compact barrel shape composed of α-helices and β-strands [10]. Many proteases in the S8 family contain one or more calcium ion binding sites to stabilize their structure [10,41]. Both 4DZT and 5WSL have two calcium ion binding sites. The three potential calcium ion binding sites in KER0199 are consistent with those confirmed by crystal structures of 1S2N. Additionally, as shown in Fig. 5, the surface electrostatic potential map indicates that only KER0199 and 1S2N have a negatively charged region(*red*)near the calcium binding site 3, which facilitates calcium ion binding.

Surface electrostatic potentials of the four proteins reveal significant differences between KER0199 and its three homologs. As shown in Fig. 5, KER0199's substrate-binding pocket is notably large and flat, with a more neutral electrostatic potential in the active site and surrounding pocket, as indicated by lighter color intensity. Weaker electrostatic interactions are suggested to play a crucial role in substrate specificity [42], which may influence the adsorption and degradation of insoluble keratin substrates. Additionally, the surface outside the substrate-binding pocket of KER0199 features several negatively charged regions (red), whereas its homologs predominantly show positively charged regions (blue). The chemical properties of surface-exposed groups in proteins are critical for enabling their functions to varying temperatures, as temperature affects water structure and, consequently, protein-water interactions [43].

3.8. Substrates docking analysis of KER0199

AlphaFold 3, with its substantially updated diffusion-based architecture, is currently one of the most accurate tools for predicting protein-ligand interactions [25]. Based on the results of substrate specificity tests, AlphaFold 3 was used to dock alpha-S1-casein (NCBI Reference Sequence: AAA30429.1), hemoglobin subunit alpha (NCBI Reference Sequence: NP_000508.1), BSA (PDB: 4F5S_A), and feather keratin (GenBank: AAA48930.1) with KER0199. an analysis of intermolecular forces was then performed on the resulting models.

A screenshot of the docking results, including AlphaFold prediction scores, is provided in the supplementary materials (see Fig. S4-S7). Notably, substrates lacking a stable 3D structure, such as feather keratin P02450, exhibit very low pTM scores (0.17 for P02450) from AlphaFold3. As a result, docking the full-length substrate with the enzyme yields correspondingly low ipTM scores. Therefore, a more detailed analysis of the models is necessary for screening. *Re*-docking individual peptide segments of the substrate that interact with the enzyme—rather than using the full-length substrate—often leads to significantly higher scores. For instance, the peptide corresponding to residues 30–37 of P02450 with KER0199 achieves an ipTM score of 0.82 and a pTM score of 0.96. Furthermore, proteases typically have multiple cleavage sites on their substrates, leading to several predicted models from AlphaFold3. Due to space constraints, Fig. 6 illustrates one interaction model for each substrate.

As demonstrated in Fig. 6, despite significant differences in the amino acid sequences of various substrates, most degradable substrates—excluding BSA—occupy the substrate-binding pocket of the KER0199 active site in a similar manner. PyMOL visualization shows that for casein, hemoglobin, P2450 interacting with KER0199, the substrate's amino acid residues tend to form anti-parallel β-sheets with the G97-G99 residues of KER0199. This β-sheet formation at the enzyme's active site is consistent with observations from crystallographic studies of keratinase fervidolysin and its N-terminal propeptide [38], as well as rMtaKer and other monomeric C-terminal extensions [40]. Correspondingly, docking studies of KER0199 with its N-terminal propeptide also yielded similar results (see Fig. S8-S9). Arnórsdóttir suggests that this interaction likely delineates substrate binding at both the unprimed and primed regions, affecting the substrate's binding efficiency and specificity [38].

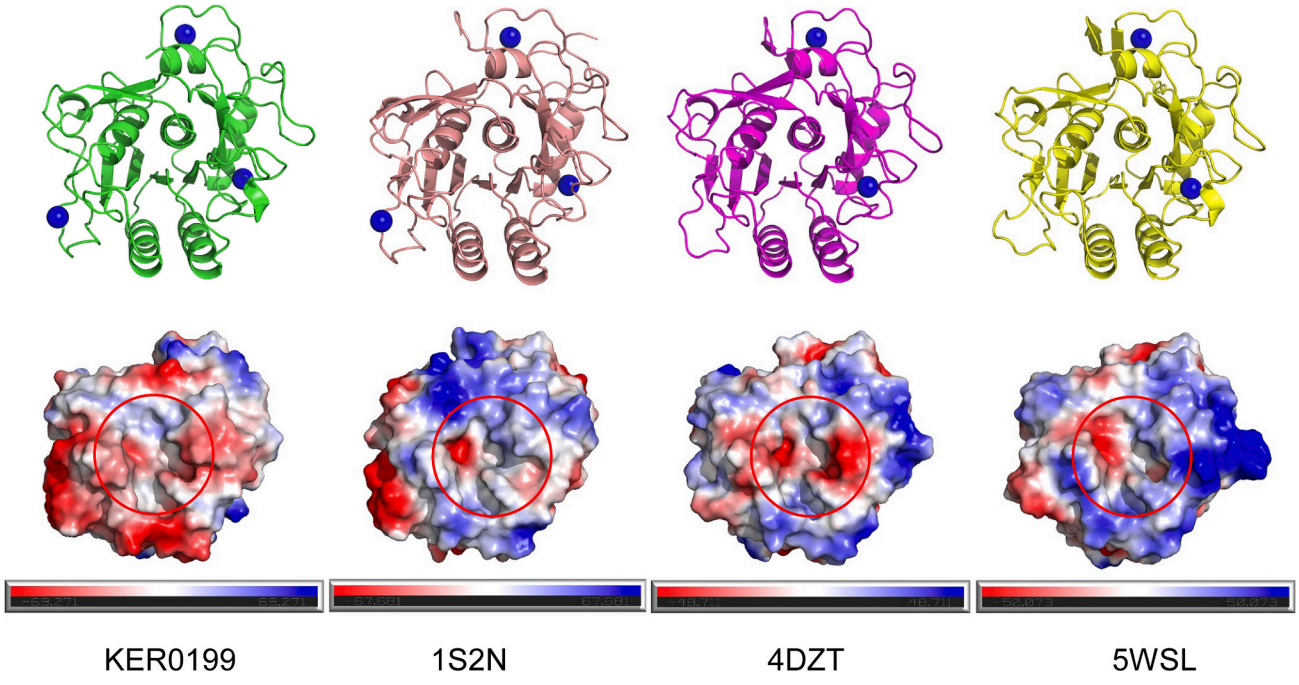

Fig. 5. Comparison of 3D Models and Surface Electrostatic Potential Maps.
Top row: Cartoon representations of the 3D models for KER0199, 1S2N, 4DZT, and 5WSL, with calcium ions shown as blue spheres.
Bottom row: Surface electrostatic potential maps. The red circles indicate the substrate binding pocket at the active sites of the enzymes.
The Figures were prepared by PyMOL.

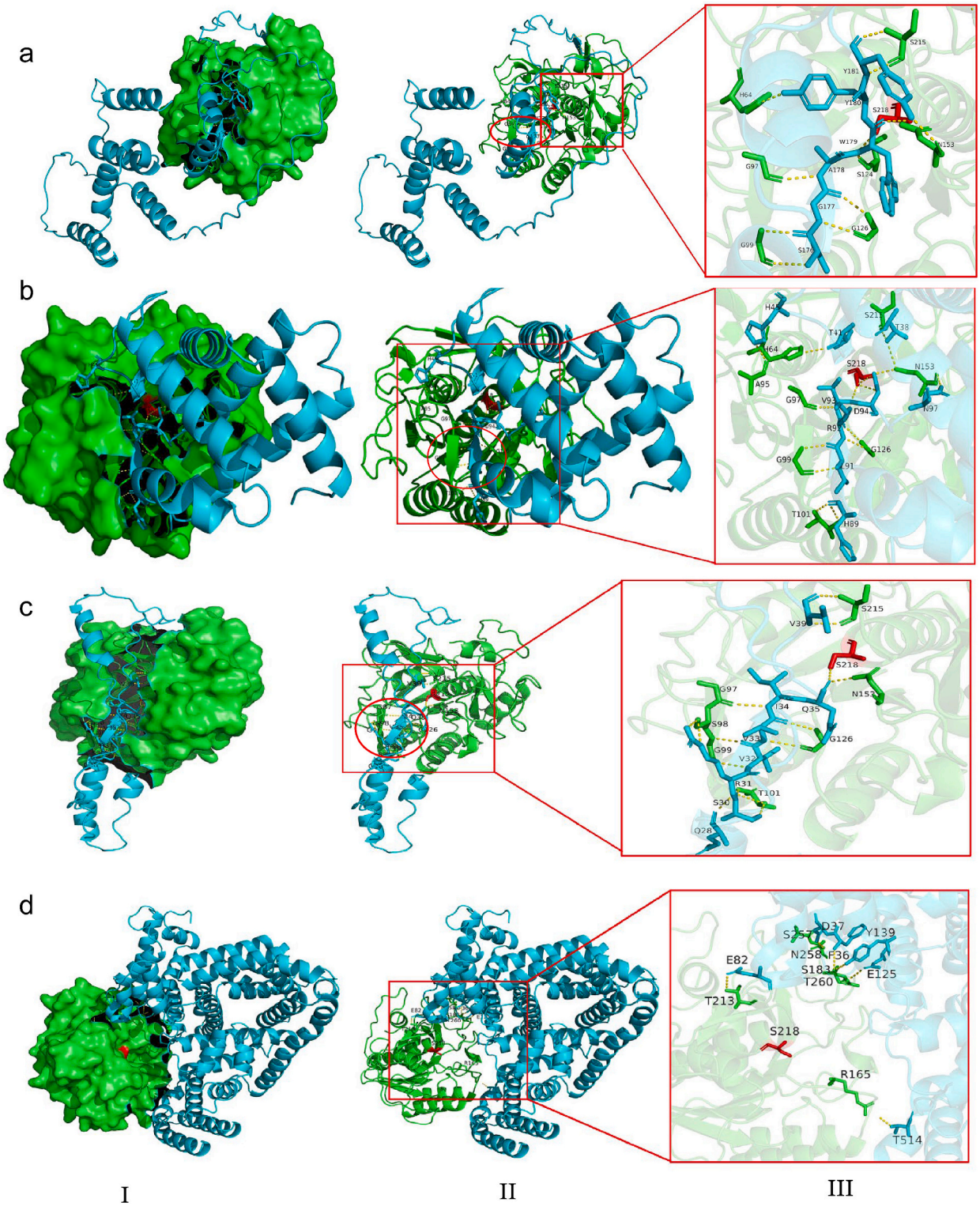

Fig. 6. Molecular Docking of KER0199 with Its Substrates.
KER0199 is depicted in green, with the catalytic triad residue S218 highlighted in red to indicate the active site. Substrates are represented in blue, including casein (a), hemoglobin (b), keratin P2450 (c), and BSA (d).
Column I: KER0199 is shown as a surface model, and substrates are depicted as cartoon representations.
Column II: Both KER0199 and substrates are shown as cartoon models. The reverse parallel β-sheets formed between KER0199 and the substrates are indicated within an oval-shaped box.
Column III: Detailed view of hydrogen bonds (depicted as yellow dashed lines) between KER0199 and substrates, which are highlighted in red boxes in Column II. Amino acid residues involved in hydrogen bonding are illustrated in stick models and labeled with single-letter codes and numbers.
The figures were prepared using PyMOL.

In addition to forming reverse parallel β-sheets, the interface between the substrates and KER0199 forms a significant number of hydrogen bonds. Despite variations in substrate molecules, the residues involved in hydrogen bond formation within the substrate-binding pocket of KER0199—namely G97, G99, S124, G126, N153, S215, and S218—are remarkably consistent. This suggests that these residues are pivotal for substrate binding and specificity. Importantly, the catalytic triad residue S218 is directly involved in these hydrogen bonds. Research indicates that non-covalent hydrogen bonds not only enhance keratinase binding to substrates [42], but low-barrier hydrogen bonds

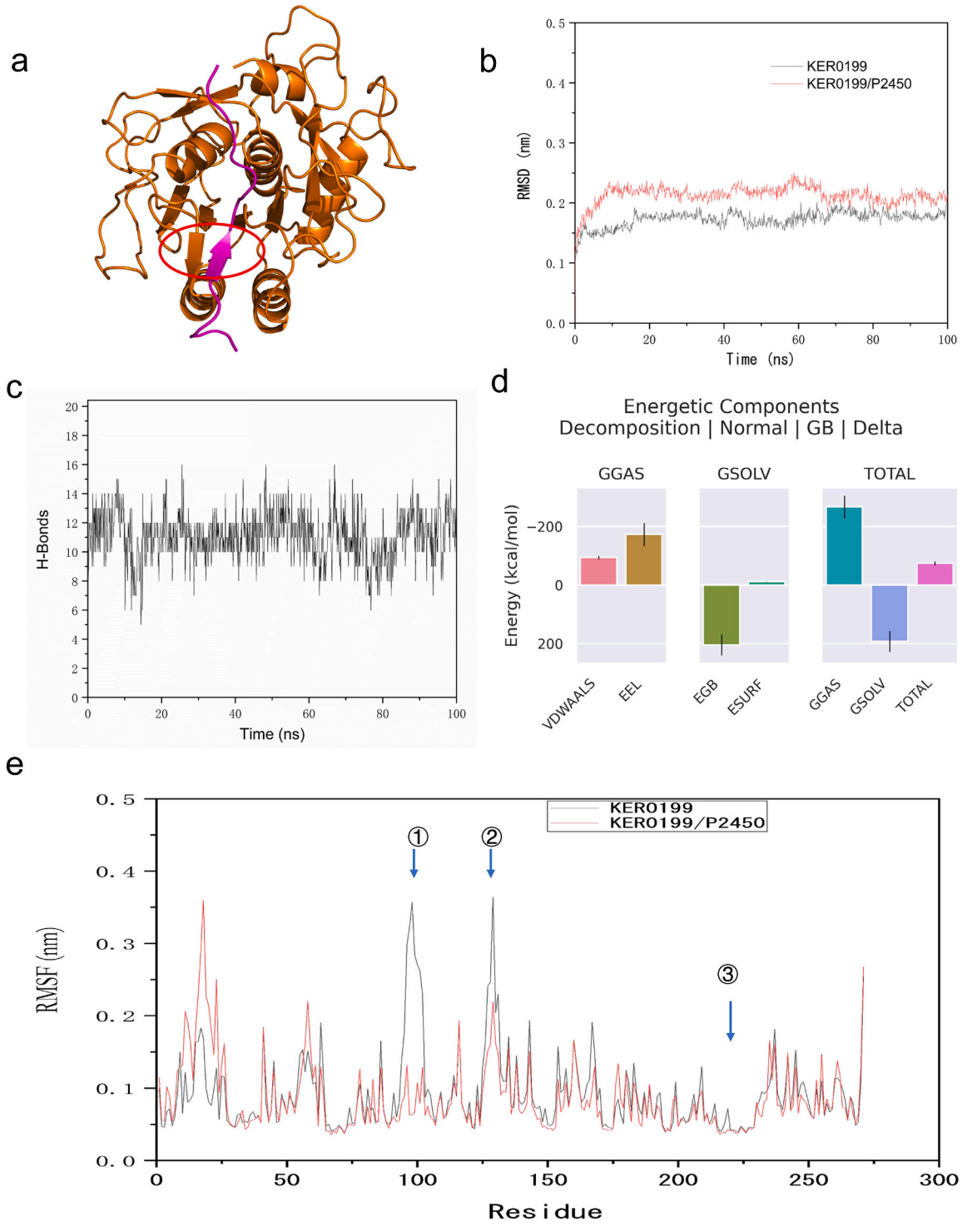

Fig. 7. Molecular Dynamics Simulation of KER0199 and P2450.
a. 3D conformation of the KER0199/P2450 complex at 100 ns, showing the inverse β-sheet structure (red circle) between KER0199 (brown) and P2450 (purple).
b. RMSD plot of KER0199 and the KER0199/P2450 complex, indicating stabilization after ~20 ns.
c. Hydrogen bond network formed between KER0199 and P2450, with ~11 hydrogen bonds fluctuating during the simulation.
d. Free energy composition of the KER0199/P2450 complex, with a total binding free energy of −74.4 ± 6.65 kcal/mol.
e. RMSF plot comparing the flexibility of monomeric KER0199 and the complex, highlighting increased flexibility in the N-terminal loop and rigidity in the substrate-binding region.

also play a crucial role in the catalytic activity of serine proteases [44–46].

Overall, the formation of reverse parallel β-sheets and numerous hydrogen bonds between the substrate and KER0199 highlights the enzyme's strong substrate binding affinity. This interaction mode likely stabilizes the substrates, especially hydrophobic keratin, enhancing its degradation performance. Conversely, BSA primarily interacts with regions outside the active site, leading to fewer hydrogen bonds and reduced binding affinity, consistent with KER0199's weak degradation of BSA. Consequently, the reduced activity against BSA underscores the enzyme's selective substrate preference and supports the accuracy of the docking predictions for alternative substrates.

3.9. Molecular dynamics (MD) simulation of KER0199 with chicken feather keratin P2450

Molecular dynamics (MD) simulations were performed on the complex formed between KER0199 and the peptide segment corresponding to residues 26–40 of chicken feather keratin P2450, based on the binding conformation of KER0199 with chicken feather keratin P2450 shown in Fig. 6c. The results are shown in Fig. 7. Fig. 7a presents the conformation extracted from the 100 ns frame of the molecular dynamics simulation trajectory. It is evident that KER0199 binds to P2450, resulting in the formation of an inverse β-sheet structure (highlighted in the red circle), which is consistent with the AlphaFold prediction. Fig. 7b compares the root mean square deviation (RMSD) of both KER0199 and the KER0199/P2450 complex, demonstrating that both systems reach equilibrium after approximately 20 ns. The KER0199/P2450 complex experiences minor fluctuations up to 64 ns, after which it stabilizes, indicating that the binding between the two is relatively stable. Fig. 7c illustrates the extensive hydrogen bond network within the complex, with approximately 11 hydrogen bonds fluctuating throughout the simulation. Fig. 7d presents the binding free energy of the complex. The gas-phase free energy (GGAS), which is negative, is calculated from van der Waals (VDWAALS) and electrostatic (EEL, EGB) interactions. Both VDWAALS <0 and EEL <0 suggest that hydrophobic interactions and electrostatic forces favor the binding. The non-polar solvation energy (ESURF) in GSOLV is negative but small, while the polar solvation energy (EGB) is positive, indicating that polar solvation is unfavorable for binding. The final total binding free energy is -74.4 ± 6.65 kcal/mol. Fig. 7e compares the root mean square fluctuation (RMSF) of the monomeric KER0199 and the KER0199/P2450 complex. Upon complex formation, KER0199 exhibits increased flexibility in the loop region formed by residues 10–20 at the N-terminus. The most significant changes are observed in the rigidification of the residue segments 96–101 (marked as ①, where the antiparallel β-sheet is formed) and 125–129 (marked as ②), both of which are located in the substrate-binding pocket, as well as Ser218 (marked as ③), the catalytic residue, which also becomes more rigid. These findings suggest that KER0199 forms a stable complex with chicken feather keratin, and that the enhanced binding affinity between the enzyme and its substrate may correlate with increased enzymatic activity.

4. Conclusions

In this study, a novel *Amycolatopsis* strain, BJA-103, distinguished by its exceptional feather-degrading capabilities, was isolated. This strain represents the second instance within the *Amycolatopsis* genus exhibiting such remarkable keratinase activity. The serine protease KER0199, derived from BJA-103, is identified as the first S8 family keratinase in the genus. KER0199 is noteworthy for its limited sequence homology with other characterized keratinases, exhibiting unique structural and functional properties. Unlike its homologs, KER0199 lacks disulfide bonds but demonstrates superior alkaline and thermal stability. Its molecular surface is predominantly negatively charged, and the substrate-binding pocket exhibits low electrostatic potential, contributing to its broad substrate range and effective degradation of both keratin and hemoglobin. The impressive performance of *Amycolatopsis* BJA-103 and its protease KER0199 highlights their considerable potential for industrial applications, particularly under demanding conditions.

Molecular docking studies have provided deeper insights into the enzyme's substrate-binding mechanism. Furthermore, the use of AI models such as AlphaFold3 has proven valuable, demonstrating that combining substrate docking with an analysis of intermolecular forces is an effective complementary approach for identifying critical amino acid residues within the substrate-binding pocket. This method enhances our understanding of the enzyme's substrate-binding mechanism and improves the prediction of its substrate specificity.

CRediT authorship contribution statement

Xia Yan: Writing – original draft, Supervision, Funding acquisition. **Hanqi Zhou:** Software, Investigation, Formal analysis. **Ruolin Wang:** Formal analysis, Data curation. **Huan Chen:** Validation, Methodology. **Bingjie Wen:** Validation, Methodology. **Mengmeng Dong:** Validation. **Quanhong Xue:** Resources. **Lianghui Jia:** Supervision, Resources, Methodology, Funding acquisition. **Hua Yan:** Writing – review & editing, Writing – original draft, Project administration, Funding acquisition, Conceptualization.

Ethics approval and consent to participate

Not applicable.

Consent for publication

Not applicable.

Funding

This work was supported by the Natural Science Basic Research Program of Shaanxi Province (grants 2021JM-087 and 2021JM-105) and NSFC Grants (31601700 and 32072477).

Declaration of competing interest

The authors declare that they have no known competing financial interests or personal relationships that could have appeared to influence the work reported in this paper.

Acknowledgments

Dr. Chuang Ma is thanked for his kind technical assistance with bioinformatics analysis.

Appendix A. Supplementary data

Supplementary data to this article can be found online at https://doi.org/10.1016/j.ijbiomac.2025.139669.

Data availability

The sequence of the protein KER0199 can be found in the GenBank repository with accession number QGA70043.1. Other data and materials can be obtained by writing to the corresponding author.

References

[1] Q. Li, Structure, application, and biochemistry of microbial keratinases, Front. Microbiol. 12 (2021) 674345, https://doi.org/10.3389/fmicb.2021.674345.
[2] S. Santha Kalaikumari, T. Vennila, V. Monika, K. Chandraraj, P. Gunasekaran, J. Rajendhran, Bioutilization of poultry feather for keratinase production and its

application in leather industry, J. Clean. Prod. 208 (2019) 44–53, https://doi.org/10.1016/j.jclepro.2018.10.076.
[3] L. Guo, L. Lu, M. Yin, R. Yang, Z. Zhang, W. Zhao, Valorization of refractory keratinous waste using a new and sustainable bio-catalysis, Chem. Eng. J. 397 (2020) 125420, https://doi.org/10.1016/j.cej.2020.125420.
[4] B. Wang, W. Yang, J. McKittrick, M.A. Meyers, Keratin: structure, mechanical properties, occurrence in biological organisms, and efforts at bioinspiration, Prog. Mater. Sci. 76 (2016) 229–318, https://doi.org/10.1016/j.pmatsci.2015.06.001.
[5] S.R. Thankaswamy, S. Sundaramoorthy, S. Palanivel, K.N. Ramudu, Improved microbial degradation of animal hair waste from leather industry using *Brevibacterium luteolum* (MTCC 5982), J. Clean. Prod. 189 (2018) 701–708, https://doi.org/10.1016/j.jclepro.2018.04.095.
[6] R. Gupta, R. Rajput, R. Sharma, N. Gupta, Biotechnological applications and prospective market of microbial keratinases, Appl. Microbiol. Biotechnol. 97 (2013) 9931–9940, https://doi.org/10.1007/s00253-013-5292-0.
[7] A.M. Abdel-Fattah, M.S. El-Gamal, S.A. Ismail, M.A. Emran, A.M. Hashem, Biodegradation of feather waste by keratinase produced from newly isolated *Bacillus licheniformis* ALW1, J. Genet. Eng. Biotechnol. 16 (2018) 311–318, https://doi.org/10.1016/j.jgeb.2018.05.005.
[8] S.C.B. Gopinath, P. Anbu, T. Lakshmipriya, T.-H. Tang, Y. Chen, U. Hashim, A. R. Ruslinda, M.K.Md. Arshad, Biotechnological aspects and perspective of microbial keratinase production, Biomed. Res. Int. 2015 (2015) 1–10, https://doi.org/10.1155/2015/140726.
[9] N.E. Nnolim, C.C. Udenigwe, A.I. Okoh, U.U. Nwodo, Microbial keratinase: next generation green catalyst and prospective applications, Front. Microbiol. 11 (2020) 580164, https://doi.org/10.3389/fmicb.2020.580164.
[10] J. Qiu, C. Wilkens, K. Barrett, A.S. Meyer, Microbial enzymes catalyzing keratin degradation: classification, structure, function, Biotechnol. Adv. 44 (2020) 107607, https://doi.org/10.1016/j.biotechadv.2020.107607.
[11] M.A. Hassan, D. Abol-Fotouh, A.M. Omer, T.M. Tamer, E. Abbas, Comprehensive insights into microbial keratinases and their implication in various biotechnological and industrial sectors: a review, Int. J. Biol. Macromol. 154 (2020) 567–583, https://doi.org/10.1016/j.ijbiomac.2020.03.116.
[12] V. Matikevičienė, D. Masiliūnienė, S. Grigiškis, Degradation of keratin containing wastes by bacteria with keratinolytic activity, Environ. Technol. Resour. Proc. Int. Sci. Pract. Conf. 1 (2015) 284, https://doi.org/10.17770/etr2009vol1.1107.
[13] Z. Wang, Y. Chen, M. Yan, K. Li, C.O. Okoye, Z. Fang, Z. Ni, H. Chen, Research progress on the degradation mechanism and modification of keratinase, Appl. Microbiol. Biotechnol. 107 (2023) 1003–1017, https://doi.org/10.1007/s00253-023-12360-3.
[14] F. Akram, A. Aqeel, M. Shoaib, I.U. Haq, F.I. Shah, Multifarious revolutionary aspects of microbial keratinases: an efficient green technology for future generation with prospective applications, Environ. Sci. Pollut. Res. 29 (2022) 86913–86932, https://doi.org/10.1007/s11356-022-23638-w.
[15] M. Yan, Y. Chen, Y. Feng, M. Saeed, Z. Fang, W. Zhen, Z. Ni, H. Chen, Perspective on agricultural industrialization: modification strategies for enhancing the catalytic capacity of keratinase, J. Agric. Food Chem. 72 (2024) 13537–13551, https://doi.org/10.1021/acs.jafc.4c03025.
[16] F. Zhu, Z. Yan, J. Dai, G. Li, Q. Xu, Y. Ma, J. Ma, N. Chen, X. Zhang, Y. Zang, Improvement in organic solvent resistance of keratinase BLk by directed evolution, J. Biotechnol. 382 (2024) 37–43, https://doi.org/10.1016/j.jbiotec.2024.01.007.
[17] M. Saeed, M. Yan, Z. Ni, N. Hussain, H. Chen, Molecular strategies to enhance the keratinase gene expression and its potential implications in poultry feed industry, Poult. Sci. 103 (2024) 103606, https://doi.org/10.1016/j.psj.2024.103606.
[18] J. Gong, J. Shi, Z. Xu, C. Su, Method for efficient heterologous expression of keratinase, CN111662908A, 2022.
[19] J. Zhang, Z. Peng, J. Chen, G. Du, X. Mao, H. Zhou, Recombinant *Bacillus subtilis* engineered bacterium capable of efficiently expressing keratinase, US 11384349B2 (2020).
[20] J. Zhang, J. Chen, Z. Fang, G. Du, C. Ren, Keratinase mutants with thermostability and catalytic activity improved, CN 106636042A (2019).
[21] T. Wannawong, W. Mhuantong, P. Macharoen, N. Niemhom, J. Sitdhipol, N. Chaiyawan, S. Umrung, S. Tanasupawat, N. Suwannarach, Y. Asami, N. Kuncharoen, Comparative genomics reveals insight into the phylogeny and habitat adaptation of novel *Amycolatopsis* species, an endophytic actinomycete associated with scab lesions on potato tubers, Front. Plant Sci. 15 (2024) 1346574, https://doi.org/10.3389/fpls.2024.1346574.
[22] F.C. Falco, R. Espersen, B. Svensson, K.V. Gernaey, A. Eliasson Lantz, An integrated strategy for the effective production of bristle protein hydrolysate by the keratinolytic filamentous bacterium *Amycolatopsis keratiniphila* D2, Waste Manag. 89 (2019) 94–102, https://doi.org/10.1016/j.wasman.2019.03.067.
[23] R. Espersen, F.C. Falco, P. Hägglund, K.V. Gernaey, A.E. Lantz, B. Svensson, Two novel S1 peptidases from *Amycolatopsis keratinophila* subsp. *keratinophila* D2^T degrading keratinous slaughterhouse by-products, Appl. Microbiol. Biotechnol. 104 (2020) 2513–2522, https://doi.org/10.1007/s00253-020-10380-x.
[24] Y. Ma, X. Ke, X. Li, W. Shu, W. Yang, Y. Liu, X. Yan, L. Jia, H. Yan, Expression and characterization of a keratinase encoding gene gm2886 in *Streptomyces pactum* ACT12 strain, Sheng Wu Gong Cheng Xue Bao 33 (2017) 1968–1978, https://doi.org/10.13345/j.cjb.170081.
[25] T. Kieser (Ed.), Practical *Streptomyces* Genetics, Innes, Norwich, 2000.
[26] K. Tamura, G. Stecher, D. Peterson, A. Filipski, S. Kumar, MEGA6: molecular evolutionary genetics analysis version 6.0, Mol. Biol. Evol. 30 (2013) 2725–2729, https://doi.org/10.1093/molbev/mst197.
[27] S. Yamamura, Y. Murakami, K. Yokoyama, E. Tamiya', Characterization of a new keratin-degrading bacterium isolated from deer Fur, (n.d.). J. Biosci. Bioeng. 93 (2002):595–600. doi:https://doi.org/10.1016/S1389-1723(02)80243-2.
[28] J. Abramson, J. Adler, J. Dunger, R. Evans, T. Green, A. Pritzel, O. Ronneberger, L. Willmore, A.J. Ballard, J. Bambrick, S.W. Bodenstein, D.A. Evans, C.-C. Hung, M. O'Neill, D. Reiman, K. Tunyasuvunakool, Z. Wu, A. Žemgulytė, E. Arvaniti, C. Beattie, O. Bertolli, A. Bridgland, A. Cherepanov, M. Congreve, A.I. Cowen-Rivers, A. Cowie, M. Figurnov, F.B. Fuchs, H. Gladman, R. Jain, Y.A. Khan, C.M. R. Low, K. Perlin, A. Potapenko, P. Savy, S. Singh, A. Stecula, A. Thillaisundaram, C. Tong, S. Yakneen, E.D. Zhong, M. Zielinski, A. Žídek, V. Bapst, P. Kohli, M. Jaderberg, D. Hassabis, J.M. Jumper, Accurate structure prediction of biomolecular interactions with AlphaFold 3, Nature 630 (2024) 493–500, https://doi.org/10.1038/s41586-024-07487-w.
[29] S. K, V. B, Y. M, Isolation and description of keratinase producing marine actinobacteria from south Indian coastal region, Afr. J. Biotechnol. 12 (2013) 19–26. doi:https://doi.org/10.5897/AJB12.2428.
[30] B. Jaouadi, B. Abdelmalek, D. Fodil, F.Z. Ferradji, H. Rekik, N. Zaraî, S. Bejar, Purification and characterization of a thermostable keratinolytic serine alkaline proteinase from *Streptomyces* sp. strain AB1 with high stability in organic solvents, Bioresour. Technol. 101 (2010) 8361–8369, https://doi.org/10.1016/j.biortech.2010.05.066.
[31] S.K. Rai, A.K. Mukherjee, Optimization of production of an oxidant and detergent-stable alkaline β-keratinase from *Brevibacillus* sp. strain AS-S10-II: application of enzyme in laundry detergent formulations and in leather industry, Biochem. Eng. J. 54 (2011) 47–56, https://doi.org/10.1016/j.bej.2011.01.007.
[32] Z. Peng, J. Zhang, G. Du, J. Chen, Keratin waste recycling based on microbial degradation: mechanisms and prospects, ACS Sustain. Chem. Eng. 7 (2019) 9727–9736, https://doi.org/10.1021/acssuschemeng.9b01527.
[33] B. Vidmar, M. Vodovnik, Microbial keratinases: enzymes with promising biotechnological applications, Food Technol. Biotechnol. 56 (2018) 312–328, https://doi.org/10.17113/ftb.56.03.18.5658.
[34] M. Sypka, I. Jodłowska, A.M. Białkowska, Keratinases as versatile enzymatic tools for sustainable development, Biomolecules 11 (2021) 1900, https://doi.org/10.3390/biom11121900.
[35] K.L. Evans, J. Crowder, E.S. Miller, Subtilisins of *Bacillus* spp. hydrolyze keratin and allow growth on feathers, Can. J. Microbiol. (2011), https://doi.org/10.1139/w00-085.
[36] G.I. Makhatadze, P.L. Privalov, Contribution of hydration to protein folding thermodynamics: I. The enthalpy of hydration, J. Mol. Biol. 232 (1993) 639–659, https://doi.org/10.1006/jmbi.1993.1416.
[37] S.E. Tork, Y.E. Shahein, A.E. El-Hakim, A.M. Abdel-Aty, M.M. Aly, Production and characterization of thermostable metallo-keratinase from newly isolated *Bacillus subtilis* NRC 3, Int. J. Biol. Macromol. 55 (2013) 169–175, https://doi.org/10.1016/j.ijbiomac.2013.01.002.
[38] J. Arnórsdóttir, M.M. Kristjánsson, R. Ficner, Crystal structure of a subtilisin-like serine proteinase from a *psychrotrophic Vibrio* species reveals structural aspects of cold adaptation, FEBS J. 272 (2005) 832–845, https://doi.org/10.1111/j.1742-4658.2005.04523.x.
[39] P.R. Green, J.D. Oliver, L.C. Strickland, D.R. Toerner, H. Matsuzawa, T. Ohta, Purification, crystallization and preliminary X-ray investigation of aqualysin I, a heat-stable serine protease, Acta Crystallogr. D Biol. Crystallogr. 49 (1993) 349–352, https://doi.org/10.1107/S0907444992012083.
[40] W.-L. Wu, M.-Y. Chen, I.-F. Tu, Y.-C. Lin, N. EswarKumar, M.-Y. Chen, M.-C. Ho, S.-H. Wu, The discovery of novel heat-stable keratinases from *Meiothermus taiwanensis* WR-220 and other extremophiles, Sci. Rep. 7 (2017) 4658, https://doi.org/10.1038/s41598-017-04723-4.
[41] S.-Q. Liu, L.-M. Liang, T. Yan, L.-Q. Yang, X.-L. Ji, J.-K. Yang, Y.-X. Fu, K.-Q. Zhang, "structural and dynamic basis of serine proteases from Nematophagous Fungi for cuticle degradation," in * pesticides in the modern world - pests control and pesticides exposure and toxicity assessment*, IntechOpen (2011), https://doi.org/10.5772/19026.
[42] Z. Fang, J. Zhang, B. Liu, G. Du, J. Chen, Insight into the substrate specificity of keratinase KerSMD from *Stenotrophomonas maltophilia* by site-directed mutagenesis studies in the S1 pocket, RSC Adv. 5 (2015) 74953–74960, https://doi.org/10.1039/C5RA12598G.
[43] C.-J. Tsai, J.V. Maizel, R. Nussinov, The hydrophobic effect: a new insight from cold denaturation and a two-state water structure, Crit. Rev. Biochem. Mol. Biol. (2002), https://doi.org/10.1080/10409230290771456.
[44] W.W. Cleland, M.M. Kreevoy, Low-Barrier Hydrogen Bonds and Enzymic Catalysis, science. 264 (1994) 1887–1890, https://doi.org/10.1126/science.8009219.
[45] P.A. Frey, S.A. Whitt, J.B. Tobin, A Low-barrier hydrogen bond in the catalytic triad of serine proteases, Science 264 (1994) 1927–1930, https://doi.org/10.1126/science.7661899.
[46] B. Dereka, Q. Yu, N.H.C. Lewis, W.B. Carpenter, J.M. Bowman, A. Tokmakoff, Crossover from hydrogen to chemical bonding, Science 371 (2021) 160–164, https://doi.org/10.1126/science.abe1951.